Applied Catalysis B: Environmental 240 (2019) 64–71

Contents lists available at ScienceDirect

Applied Catalysis B: Environmental

journal homepage: www.elsevier.com/locate/apcatb

Salt-template-assisted construction of honeycomb-like structured g-C_3N_4 with tunable band structure for enhanced photocatalytic H_2 production

Fan Yang[a,b], Dongzhi Liu[b,c,**], Yunxiang Li[d,e], Lijun Cheng[a], Jinhua Ye[a,b,d,e,*]

[a] TJU-NIMS International Collaboration Laboratory, School of Materials Science and Engineering, Tianjin University, Tianjin 300072, PR China
[b] Collaborative Innovation Center of Chemical Science and Engineering, Tianjin University, Tianjin 300072, China
[c] School of Chemical Engineering and Technology, Tianjin University, Tianjin 300072, China
[d] Photocatalytic materials group, International Center for Materials Nanoarchitectonics (WPI-MANA), National Institute for Materials Science, 1-1 Namiki, Tsukuba, Ibaraki 305-0044, Japan
[e] Graduate School of Chemical Science and Engineering, Hokkaido University, Sapporo 060-0814, Japan

ARTICLE INFO

Keywords:
Photocatalytic water splitting
g-C_3N_4
Honeycomb-like structure
Cyano group defect
Na ion doping

ABSTRACT

Honeycomb-like structured graphitic carbon nitride (g-C_3N_4) with tunable band structure was prepared through a one-step salt-template assisted approach. The honeycomb structure, cyano group defects and Na ion doping result in enhanced light absorption, improved photoexcited charge carrier separation, and up-shift of conduction band. As a consequence, the photocatalytic H_2 evolution rate is about 5.2 times higher than that of the pristine graphitic carbon nitride. This newly developed approach provides a promising way to modify other functional materials through nanostructure design coupled with electronic modulation strategy simultaneously.

1. Introduction

Semiconductor photocatalysis has attracted much attention as a potential solution to solve the energy crisis and environmental problem [1–8]. Photocatalytic H_2 evolution is a promising way to develop clean and sustainable energy [1–5]. Among various photocatalysts, graphitic carbon nitride (g-C_3N_4), a metal-free polymer organic semiconductor has attracted plenty of research interest owing to its excellent chemical and thermal stability, nontoxic, simple synthesis and low cost [9–17]. However, pristine graphitic carbon nitride (PCN) prepared by direct polycondensation of precursors suffers from inefficient utilization of visible light and fast photogenerated charge carrier recombination rate, resulting in poor photocatalytic activity. In order to improve the photocatalytic activity of pristine g-C_3N_4, various modification methods, such as exfoliation [18–20], coupling with other semiconductors [21–24], nanostructure design [25–32], and electronic structure modulation strategy (such as elemental and molecular doping [33–37] and defect engineering [38–45]) have been developed. In addition, the photocatalytic performance can also be dramatically enhanced by selecting a low-cost cocatalyst instead of Pt such as two-dimensional Ti_2C and VS_2 [46,47]. It is well known that the morphology of photocatalysts plays an important role in its photocatalytic performance. The construction of honeycomb structure is helpful to enhance light absorption through the multiple scattering of the incident light and accelerate mass diffusion of reactant molecules, thus improving the photocatalytic performance [25,48–50]. Nanostructure design is an effective way to obtain g-C_3N_4 with ordered nanostructure via soft or hard template methods. In terms of the soft template approach, the carbon residual generated from the surfactant and block copolymer soft template cannot be removed. Moreover, the excessive carbon residual may offer more potential recombination sites, which is adverse to the photocatalytic activity [51]. In regard to the hard-template approach, silica nanoparticles, mesoporous silica, and anodic alumina oxide are the commonly-used hard templates and poisonous etchant such as HF or NH_4HF_2 is always required to remove the templates, which is not environmentally friendly [11]. It is highly desirable to fabricate honeycomb-like structured g-C_3N_4 via an environmental friendly way.

The electronic structure of g-C_3N_4 has a very important influence on the light absorption and band structure, which significantly determine the photocatalytic performance. The electronic modulation strategy (doping and defect engineering) provides a facile route to enhance light absorption and tune band structure by modulating the electronic structure. It is reported that the conduction band (CB) and valence band (VB) potential of g-C_3N_4 can be tuned facilely by controlling the Na ion

* Corresponding author at: TJU-NIMS International Collaboration Laboratory, School of Materials Science and Engineering, Tianjin University, Tianjin 300072, PR China.
** Corresponding author at: School of Chemical Engineering and Technology, Tianjin University, Tianjin 300072, China.
E-mail addresses: dzliutju@163.com (D. Liu), Jinhua.YE@nims.go.jp (J. Ye).

https://doi.org/10.1016/j.apcatb.2018.08.072
Received 12 June 2018; Received in revised form 10 August 2018; Accepted 28 August 2018
Available online 29 August 2018
0926-3373/

doping concentration [52–54]. Recently, it is demonstrated that the introduction of cyano group defects can narrow the band gap to enhance light absorption and improve the photogenerated charge carrier separation [40]. Additionally, cyano group defects can also act as the photocatalytically relevant sites [41]. However, a facile way to prepare honeycomb-like structured g-C_3N_4 with tunable band structure simultaneously has been barely reported.

In this article, honeycomb-like structured g-C_3N_4 with tunable band structure was fabricated through one-step calcination by using water-soluble NaCl cubes as the template. The morphology and band structure can be tuned by controlling the ratio of NaCl: DCDA. When the ratio of NaCl: DCDA reaches to 10, the photocatalytic performance is 5.2 times as high as that of the pristine g-C_3N_4, which is attributed to the enhanced light absorption, efficient photoexcited charge carrier separation and negative shift of conduction band. This work is expected to provide a strategy to modify g-C_3N_4 by combining nanostructure design and electronic modulation at the same time.

2. Experimental section

2.1. Synthesis of pristine g-C_3N_4

In a typical procedure, 4.5 g dicyandiamide (DCDA) was placed into a crucible with a cover and calcined at 550 °C for 2 h with a ramping rate of 5 °C /min. The as-obtained product was named as PCN.

2.2. Synthesis of honeycomb-like structured g-C_3N_4 with tunable band structure

4.5 *g* dicyandiamide was dissolved into 500 mL ethanol and a certain amount of NaCl saturated aqueous solution was then injected drop by drop into dicyandiamide ethanol solution under constant stirring vigorously. The ethanol and water were removed by rotary evaporation and the obtained powder was calcined at 550 °C for 2 h with a ramping rate of 5 °C/min. After the calcination, the samples were added into deionized water under constant stirring. After the mixture was stirred for 1 h, the product was collected through centrifugation, washed with deionized water several times to remove any water-soluble impurity and dried in vacuum. The samples synthesized with various amounts of NaCl (the molar ratio of NaCl: DCDA = 1:1, 3:1, 5:1, 10:1, and 15:1) were noted as CN-1, CN-3, CN-5, CN-10, and CN-15, respectively. The m-CN-10 as a control was prepared by just mixing DCDA with NaCl (the molar ratio of NaCl: DCDA = 10) and heating to 550 °C for 2 h with a ramping rate of 5 °C /min. After the calcination, the sample was treated by the same procedure for CN-10 mentioned above.

2.3. Characterization

X-ray diffraction (XRD) measurements were carried out on a Bruker D8 Focus Diffraction System with Cu Kα radiation. Scanning electron microscopy (SEM) images were obtained using a Hitachi S-4800 scanning electron microscope at an accelerating voltage of 3 kV and energy dispersive spectrometer (EDS) mapping was measured using a Thermo Scientific energy dispersive spectroscopy. UV–vis diffuse reflectance spectra (DRS) were obtained on a UV–vis spectrometer (UV-2700, Shimadzu, Japan) using $BaSO_4$ as the reference. X-ray photoelectron spectroscopy (XPS) examinations were carried out to analyze the composition, chemical state and valence band position of the samples on a PHI-1600 X-ray photoelectron spectrometer using Al Kα radiation. The steady photoluminescence (PL) spectra and time-resolved fluorescence spectra were recorded on a Jobin Yvon Fluorolog 3–21 fluorescence spectrometer. The specific surface area was measured at 77 K using an Autosorb-iQ2-MP apparatus. Fourier transform infrared (FTIR) spectra were measured on a Thermo Scientific Nicolet 6700 spectrophotometer. The solid ^{13}C MAS nuclear magnetic resonance (NMR) spectra of PCN and CN-10 were recorded on an Infinity Plus 300 spectrometer.

2.4. Fabrication of electrodes and photoelectrochemical tests

Before fabricating working electrodes, the F-doped tin oxide (FTO) substrates were cleaned through ultrasonication in absolute ethanol, acetone and absolute ethanol for 20 min sequentially. To fabricate working electrodes, 4 mg of sample was dispersed in 4 mL absolute ethanol and the as-prepared slurry was spread on a FTO substrate (1 × 1 cm^2) and subsequently calcined at 300 ℃ for 2 h. The working electrodes studied are with a similar loading amount. The electrochemical impedance spectroscopies (EIS) and transient photocurrent response studies were investigated in a conventional three-electrode cell with an Ag/AgCl reference electrode, a working electrode, and a Pt counter electrode. Na_2SO_4 aqueous solution (0.5 M) was used as the electrolyte solution. A 300 W Xenon lamp with a UV-cutoff filter (λ > 400 nm) was used as the light source. The Nyquist plots were recorded at 1.0 V bias potential versus Ag/AgCl over the frequency range from 1 MHz to 0.1 Hz. The transient photocurrent response tests were performed at an applied 1.0 V potential versus Ag/AgCl.

2.5. Photocatalytic activity tests

The photocatalytic H_2 production tests were performed in a Pyrex glass reaction cell connected to a gas-closed system. In a typical procedure, 50 mg of photocatalysts was added into 270 mL 25 vol% of lactic acid aqueous solution. 3 wt% Pt was in situ photodeposited on the surface of photocatalysts by irradiation with a 300 W Xenon lamp for 2 h. Prior to the irradiation, the reaction cell was evacuated several times to remove the air completely. Then the aqueous dispersion of photocatalysts was irradiated under a 300 W Xenon lamp equipped with a UV-cutoff filter (λ > 400 nm). The evolved H_2 was analyzed by an online Shimadzu GC-2014C gas chromatograph equipped with a thermal conductivity detector. The apparent quantum yield (AQY) was measured by using 300 W Xenon lamp with a water filter and bandpass filter (420 nm). A radiant power energy meter (AvaSolar-1) was used to measure the number of incident photons. The AQY was calculated by using the following equations.

$$AQY\,(\%) = \frac{\text{number of reacted electrons}}{\text{number of incident photons}} \times 100\%$$

$$= \frac{\text{number of hydrogen molecules} \times 2}{\text{number of incident photons}} \times 100\%$$

3. Results and discussion

3.1. Characterization of honeycomb-like structured graphitic carbon nitride with tunable band structure

The preparation process of honeycomb-like structured graphitic carbon nitride with tunable band structure is shown in Fig. 1. XRD characterization was performed to investigate the crystal structure of PCN and CN samples. As presented in Fig. 2, the XRD pattern of PCN shows two characteristic peaks located at around 13.0° and 27.4°, corresponding to the 100 and 002 crystal planes of g-C_3N_4, respectively. As for the CN samples, the 002 peak shifts to a larger angle, suggesting a decreased layer distance. In addition, the peak intensity decreases and the peak is broadened with the increase of the molar ratio of NaCl: DCDA, indicating the decrease of crystallinity caused by the incorporation of Na [55], after modification.

The morphology of PCN and CN was observed through the typical SEM images. As shown in Fig. 3a and Fig. S1a, the PCN exhibits a dense irregular morphology which is composed of massive lamellar structures. The morphology of CN samples varies with the molar ratio of NaCl: DCDA. When the molar ratio of NaCl: DCDA is 1:1, some holes

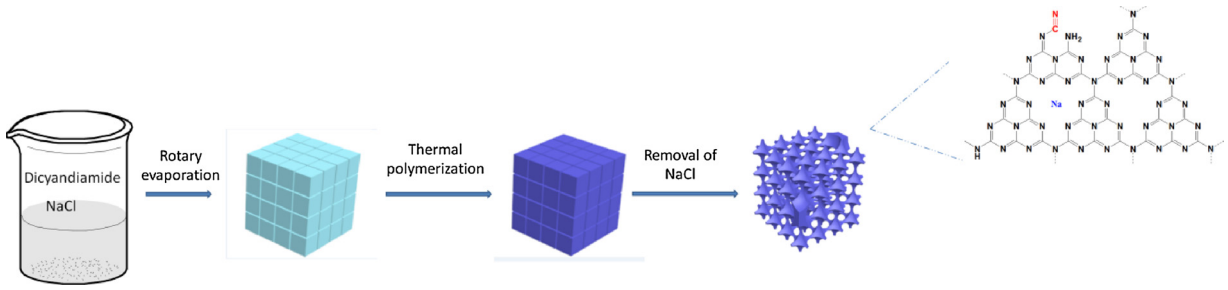

Fig. 1. Schematic illustration of preparation process of honeycomb-like structured g-C_3N_4 with tunable band structure.

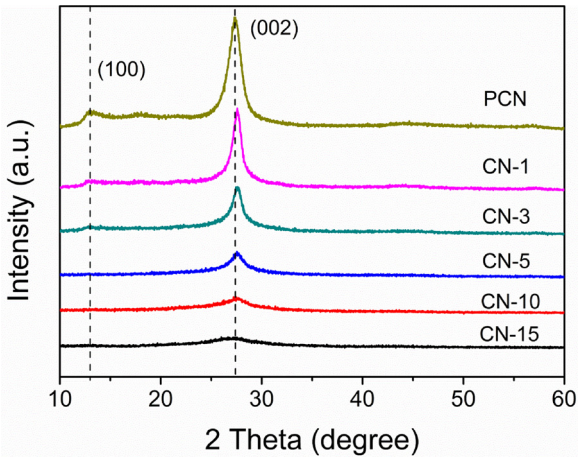

Fig. 2. XRD patterns of PCN and all the CN samples.

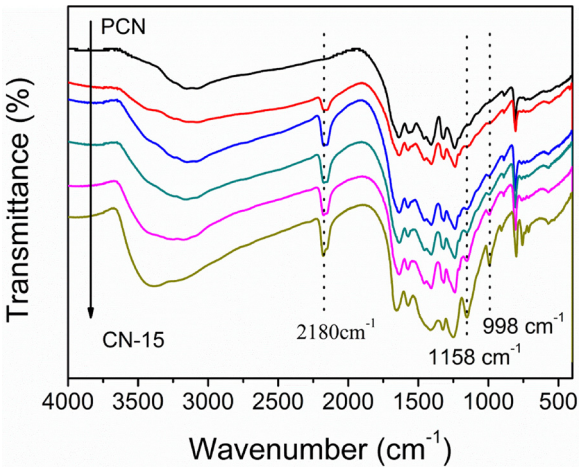

Fig. 4. FTIR spectra of PCN and all the CN samples.

appear after calcination and removal of NaCl cubes, which is formed by injecting the NaCl saturated aqueous solution into ethanol solution. The diameter of the holes is in the range of several hundred nanometers to several micrometers, which is close to the size of NaCl cubes (Fig. S1b). The number of holes increases and the size becomes larger after increasing the molar ratio of NaCl: DCDA to 3:1. Honeycomb-like structured g-C_3N_4 is observed upon increasing the ratio of NaCl: DCDA to 5 and 10. However, no honeycomb-like structure can be observed for m-CN-10 (Fig. S1c), which was prepared by using NaCl without further treatment instead of NaCl cubes as the template. This is because the size of NaCl without further treatment is so large (Fig. S1d). The honeycomb-like structure is destroyed after further increasing the molar ratio of NaCl: DCDA to 15. The phenomenon of varying morphology with the increase of NaCl usage is explained as follows. When the ratio of NaCl: DCDA is 1:1 and 3:1, NaCl cubes can be dispersed loosely in DCDA. Holes appear after removing the NaCl templates and are separated with each other. When the ratio of NaCl: DCDA reaches to 5:1 and 10:1, the NaCl cubes are closely assembled and DCDA fills the gaps of the NaCl templates after the rotary evaporation. Thus, honeycomb-like structure is obtained after calcination and removal of the NaCl templates. When the ratio of NaCl: DCDA further increases to 15:1, the wall is so thin that the honeycomb-like structure collapses finally after removing the NaCl templates. BET analysis was carried out to examine the effect of NaCl usage on the specific surface area of the modified samples. As shown in Fig. S2, the addition of NaCl templates presents little effect on the surface area of the modified samples since the size of NaCl cubic templates is so large.

The FTIR spectra were measured to analyze the chemical structure of PCN and CN shown in Fig. 4. The peaks centered at 810 cm^{-1},

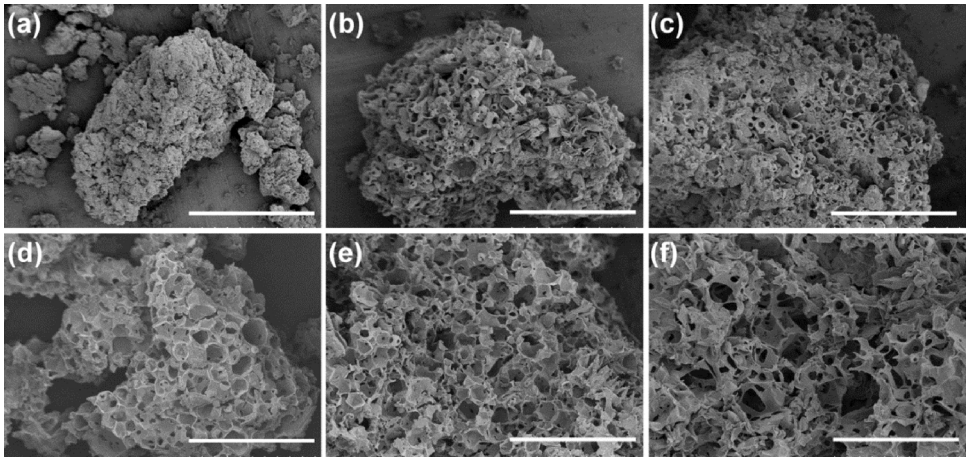

Fig. 3. SEM images of (a) PCN, (b) CN-1, (c) CN-3, (d) CN-5, (e) CN-10, and (f) CN-15.The scale bars represent 50 μm.

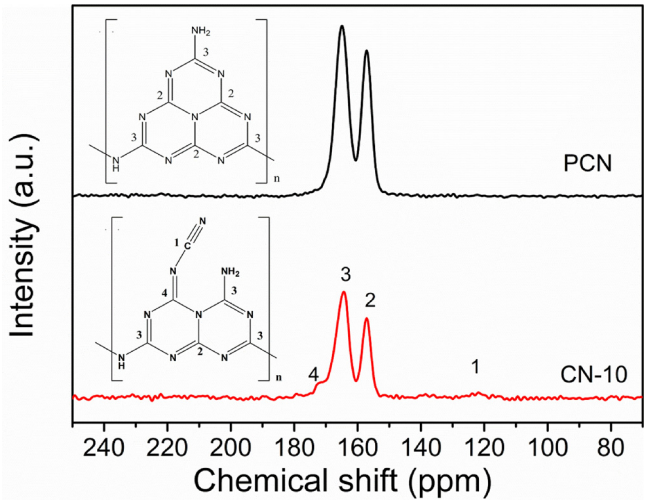

Fig. 5. Solid-state ^{13}C magic angle spinning (MAS) NMR spectra of PCN and CN-10.

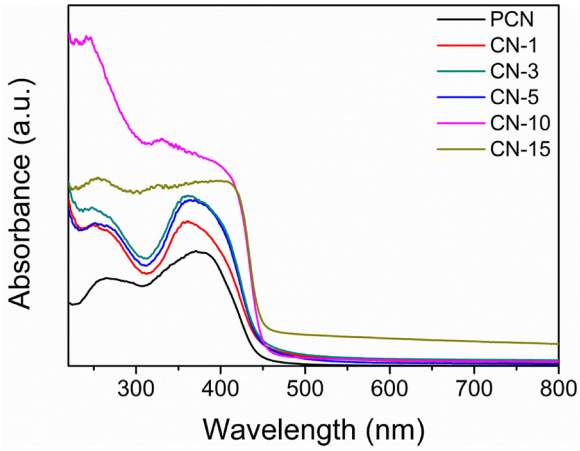

Fig. 7. UV–vis absorption spectra of PCN and all the CN samples.

regions in the range of 1200-1700 cm^{-1} and 3000-3700 cm^{-1} are assigned to the bending mode of heptazine ring, stretching vibration modes of C–N heterocycles and N—H, respectively. As for CN, a new strong peak located around 2180 cm^{-1} is found, which is attributed to cyano group (⁻ C ≡ N), generated by the catalytic pyrolysis of g-C_3N_4 in the presence of NaCl [56,57]. Moreover, new peaks located at around 998 cm^{-1} and 1158 cm^{-1} appear, corresponding to hydroxyl group [58,59].

In order to gain further insight into the generated cyano group, solid-state ^{13}C magic angle spinning (MAS) NMR spectra were measured. As presented in Fig. 5, both NMR spectra of PCN and CN-10 show two strong peaks at around 157.2 and 164.9 ppm, which are ascribed to the C (2) atoms of (CN_3) and C (3) atoms of [$CN_2(NH_X)$], respectively. As for CN-10, two new peaks appear at ca 122.1 and 172.1 ppm corresponding to C (1) atom in cyano groups and C (4) atom close to cyano

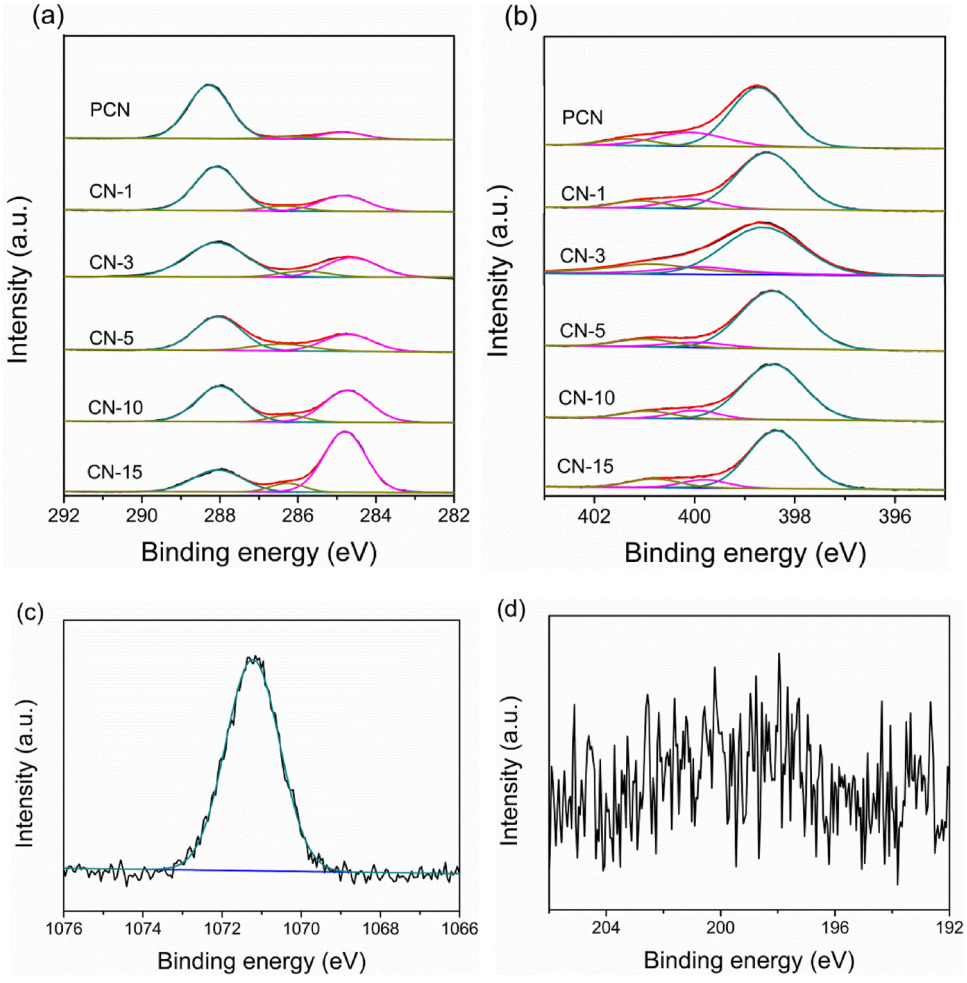

Fig. 6. (a) C 1 s and (b) N 1 s high-resolution spectra of PCN and all the CN samples. (c) Na 1 s and (d) Cl 2p high-resolution spectra of CN-10.

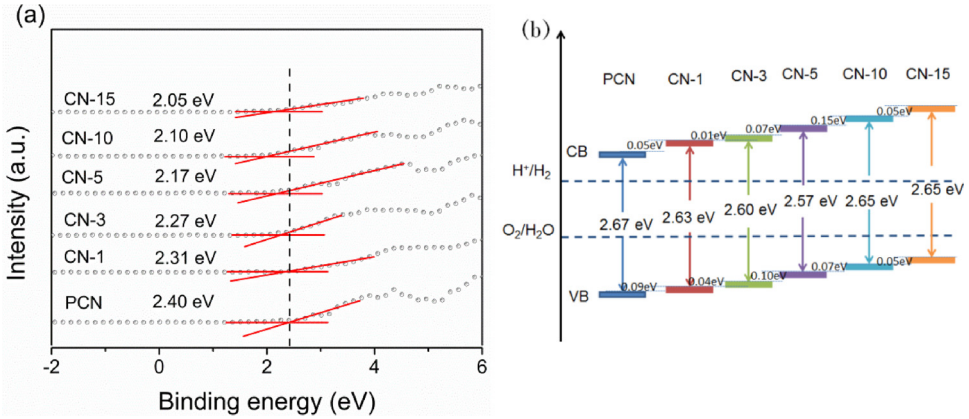

Fig. 8. (a) Valence band XPS of PCN and all the CN samples. (b) Schematic illustration of band structure of PCN and all the CN samples.

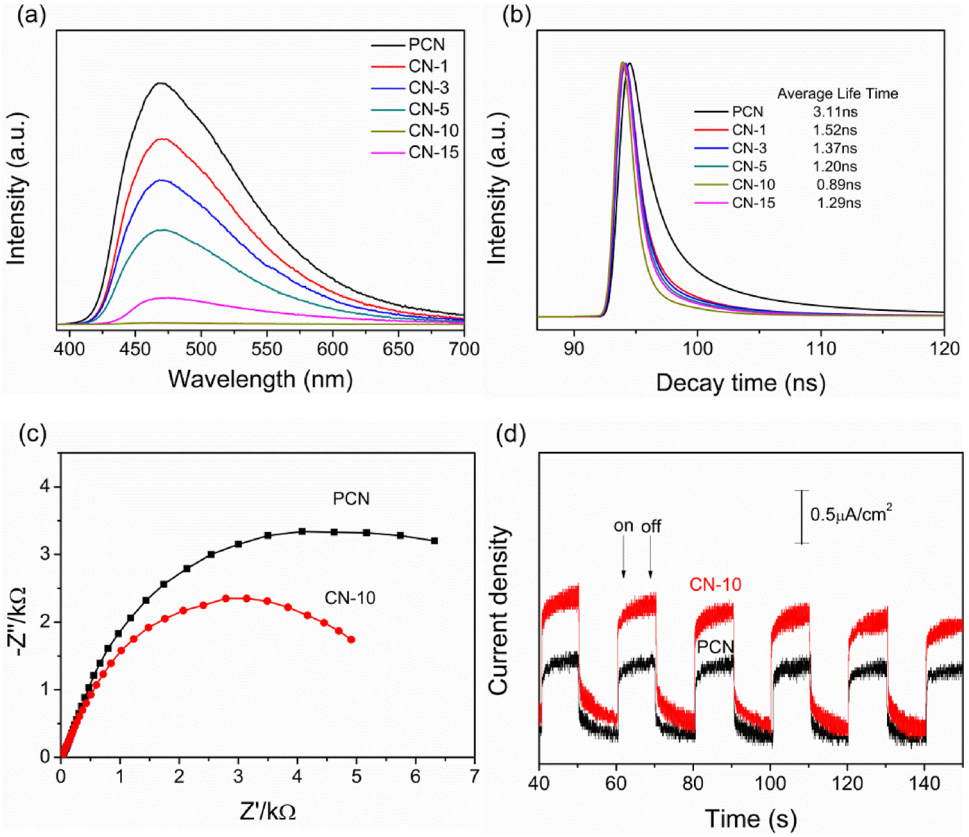

Fig. 9. (a) Steady PL spectra and (b) Time-resolved PL decay spectra of PCN and all the CN samples. (c) EIS Nyquist plots and (d) Transient photocurrent responses of PCN and CN-10.

groups [38]. The NMR results further confirm that cyano groups are formed in the CN samples, which is consistent with the FTIR result.

XPS analysis was performed to investigate the surface chemical bonding of the samples. As shown in Fig. 6a, the deconvolution of the C 1 s peak produces three peaks located at about 288.3, 286.2, and 284.8 eV, which can be ascribed to sp^2-hybridized C atom attached to N in the aromatic ring (N = C-$(N)_2$), C–NH_X species on the edge of aromatic ring and carbon impurities, respectively. In addition, the signal of the peak at about 286.2 eV of CN-10 is intensified compared with PCN, which is ascribed to the generated cyano groups due to the similar binding energy with C–NH_x [38,42]. The high-resolution N 1 s spectra (Fig. 6b) can also be deconvolved into three peaks at 401.3, 400.1, and 398.7 eV, which is assigned to amino functional groups (C–N-H), bridging N atoms in N-$(C)_3$ (N_{3C}), and sp^2-hybridized N atom attached to C in the aromatic ring (N_{2C}) respectively. The signal of Na is identified in the modified samples. As shown in the Na 1 s high-resolution spectra (Fig. 6c), the peak located at 1071.2 eV is in accordance with the reported binding energy of NaN_3, indicating that Na ions are coordinated into the C–N rings with threefold N-bridge linking the triazine units of the modified g-C_3N_4 [52,60]. Moreover, Na ion is distributed evenly in the honeycomb structure, which is confirmed by the EDS mapping (Fig. S3). And Na doping concentration of all the samples was determined through the EDS analysis (Table S1). In addition, there is little signal of Cl in the Cl 2p high-resolution spectra (Fig. 6d). Fig. S4 shows the O 1 s high-resolution spectra of PCN and CN-10.The peak at around 532.6 eV is attributed to surface adventitious species. After modification by NaCl, a new peak located at 535.2 eV appears, which is assigned to C—OH species. The binding energy of C 1 s, N 1 s, and O 1 s

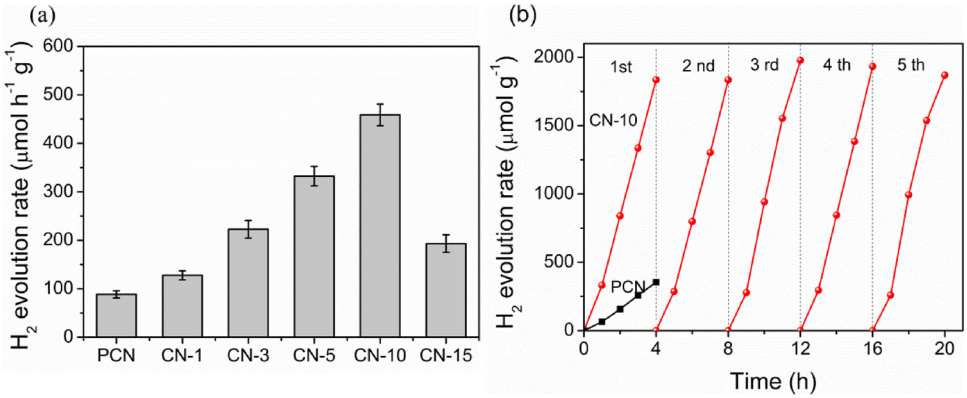

Fig. 10. (a) Photocatalytic H_2 evolution rate of PCN and all the CN samples. (b) Photocatalytic H_2 evolution cycling test of CN-10.

is lower than that of PCN, which is due to the strong interplay between Na and N [58].

The light harvesting property was investigated by DRS. The absorption edge of all the CN samples exhibits red shift and the light absorption intensity is enhanced compared with PCN, which is due to regenerated cyano group defects, Na ion doping, and multiple reflections effect within the honeycomb-like structure (Fig. 7). The light absorption intensity increases with the mole ratio of NaCl: DCDA. When the mole ratio of NaCl: DCDA reaches to 10, the light absorption intensity achieves the maximal value. Interestingly, a broader and stronger absorption tail prolonging to 800 nm can be clearly observed for CN-15, which may be caused by introducing substantial cyano group defects and Na ion doping. The corresponding band gap of PCN and CN is shown in Fig S5.

To further investigate the effect of cyano group defects and Na ion doping on band structure of CN samples, valence band (VB) XPS were carried out to determine the VB level and present in Fig. 8a. Then the conduction band (CB) can be calculated according to the corresponding band gap. A schematic illustration describing the band structure can be drawn by combining with the VB and CB potential, which is shown in Fig. 8b. The CB potential of CN samples is more and more negative compared with that of PCN with increasing the ratio of NaCl: DCDA, leading to a stronger driving force to produce H_2 in terms of thermodynamic requirements for photocatalytic reactions.

PL spectra were measured to investigate the photogenerated charge carrier separation efficiency of photocatalysts. As shown in Fig. 9a, the PL intensity of CN samples decreases sharply after treatment by NaCl, suggesting the combination of photoexcited charge carriers is much depressed. As for CN-15, the PL intensity is a little stronger than CN-10. This may be because the excessive cyano group defects seem to act as the recombination centers. In addition, the PL lifetime of photoexcited charge carriers was measured by the time-resolved PL spectra. The average lifetime is calculated by tri-exponential fitting and shown in Fig. 9b. The detailed lifetime and corresponding percentages are listed in Table S2. The average lifetime decreases from 3.11 ns (PCN) to 0.89 ns (CN-10). In addition, it can be obviously observed that the EIS Nyquist plot arc radius of CN-10 is smaller than that of PCN (Fig. 9c). Moreover, transient photocurrent response tests were carried out during repeated on/off cycles of light illumination. As shown in Fig. 9d, the photocurrent density of CN-10 is higher than that of PCN, indicating that more efficient photoinduced electron-hole separation is achieved by CN-10 than PCN, which lends support to the analysis of PL and EIS results.

3.2. Photocatalytic H_2 evolution production and mechanism of photocatalytic enhancement

The photocatalytic activity of the as-prepared samples was evaluated by H_2 production in a water/lactic acid solution under visible light irradiation. The activity of CN-10 is highest among the samples without the addition of Pt cocatalyst (Fig. S6). After the addition of Pt cocatalyst, the photocatalytic performance of all the samples is significantly improved. As shown in Fig. 10a, the photocatalytic performance of CN samples is remarkably enhanced after the modification with respect to PCN. The highest photocatalytic H_2 production activity (459 $\mu mol\, h^{-1}\, g^{-1}$) is achieved with CN-10, which is about 5.2 times higher than that of PCN with the apparent quantum efficiency of 2.2% (420 nm). A depressed photocatalytic activity is observed for CN-15 compared with CN-10 but is still higher than PCN, which may be caused by the deformation of the honeycomb-like structure, excessive cyano group defects and Na ion doping. As we all know, the stability of photocatalysts is also very important for its practical application. The photocatalytic stability was investigated through a cycling experiment. As shown in Fig. 10b, the high photocatalytic performance can be maintained after the five cycles'experiment. Moreover, the morphology exhibits no obvious collapse (Fig. S7a) and XRD pattern (Fig. S7b) is almost unchanged after the cycle experiment, indicating the good photocatalytic stability.

The reasons for the enhanced photocatalytic performance are analyzed as follows. The photocatalytic performance is usually influenced by surface area, crystallinity, morphology, and band structure of the photocatalysts. The surface area shows a little increase and the crystallinity decreases after the modification, indicating that these are not the key factors for improving the photocatalytic activity. To exclude the influence of hydroxyl group on the photocatalytic performance, hydroxyl group was wiped off by immersing CN-10 into dilute hydrochloric acid for one hour according to the report by Wang [61] and the as-obtained sample was named as H-CN-10. As shown in Fig. S8a, The FTIR peaks of hydroxyl group located at around 998 cm^{-1} and 1158 cm^{-1} disappear, suggesting that hydroxyl group was indeed wiped off. The photocatalytic activity of H-CN-10 is about the same of CN-10 (Fig. S8b), illustrating hydroxyl group does not play an important role in improving the photocatalytic activity of CN-10 herein, which is different from other reports [58,61]. This is because the photocatalytic H_2 production evaluation of CN-10 was conducted by using 25 vol% lactic acid as a sacrificial electron donor, in which hydroxyl group of CN-10 can also be wiped off by lactic acid. In order to illustrate the influence of honeycomb-like morphology on the photocatalytic performance, m-CN-10 as a control was prepared by using NaCl without further treatment as a template. As shown in Fig. S9a, the light absorption property of m-CN-10 is similar with CN-10 but the intensity decreases, which is due to lack of multiple scattering caused by the honeycomb-like structure compared with CN-10. The absorption band edge of m-CN-10 exhibits red shift and enhanced light absorption compared with PCN, which is caused by cyano group defects and Na ion doping. The photocatalytic performance of m-CN-10 is 3.3 times higher than that of PCN and 0.64 fold of that of CN-10 (Fig. S9b). In other words, the honeycomb-like structure, cyano group defects and Na ion doping

improve the photocatalytic activity simultaneously, which is explained as follows. Firstly, the honeycomb-like structure, cyano group defects and Na ion doping are beneficial to enhance light absorption due to the multiple reflections effect and red shift of absorption edge. Secondly, improved photoexcited charge carrier separation is achieved after the modification, which is confirmed by the PL and EIS results. Lastly, negative-shift of conduction band after the modification indicates stronger reducibility, which is helpful for the H_2 evolution reaction.

4. Conclusion

In summary, an environmentally friendly method was developed to fabricate honeycomb-like structured g-C_3N_4 with tunable band structure simultaneously. The modified g-C_3N_4 possessed 5.2-fold higher photocatalytic H_2 production activity of the pristine g-C_3N_4, which is ascribed to the enhanced visible light absorption, efficient charge carrier separation, and up-shift conduction band. Moreover, the honeycomb-like structure also benefits the reactant transfer. It is expected that this strategy to modify g-C_3N_4 by combining nanostructure design and electronic structure modulation can be applied to fabricate other functional materials.

Acknowledgements

This work received financial support fromthe National Natural Science Foundation of China (21633004), and the National Basic Research Program of China (973 Program, No. 2014CB239301).

Appendix A. Supplementary data

Supplementary material related to this article can be found, in the online version, at doi:https://doi.org/10.1016/j.apcatb.2018.08.072.

References

[1] H. Tong, S. Ouyang, Y. Bi, N. Umezawa, M. Oshikiri, J. Ye, Nano-photocatalytic materials: possibilities and challenges, Adv. Mater. 24 (2012) 229–251.
[2] F.E. Osterloh, Inorganic nanostructures for photoelectrochemical and photocatalytic water splitting, Chem. Soc. Rev. 42 (2013) 2294–2320.
[3] A. Kudo, Y. Miseki, Heterogeneous photocatalyst materials for water splitting, Chem. Soc. Rev. 38 (2009) 253–278.
[4] J. Qi, W. Zhang, R. Cao, Solar-to-Hydrogen energy conversion based on water splitting, Adv. Energy Mater. 8 (2018) 1701620.
[5] Z. Zou, J. Ye, K. Sayama, H. Arakawa, Direct splitting of water under visible light irradiation with an oxide semiconductor photocatalyst, Nature 414 (2001) 625–627.
[6] S. Dong, X. Ding, T. Guo, X. Yue, X. Han, J. Sun, Self-assembled hollow sphere shaped Bi_2WO_6/RGO composites for efficient sunlight-driven photocatalytic degradation of organic pollutants, Chem. Eng. J. 316 (2017) 778–789.
[7] S. Dong, L. Xia, T. Guo, F. Zhang, L. Cui, X. Su, D. Wang, W. Guo, J. Sun, Controlled synthesis of flexible graphene aerogels macroscopic monolith as versatile agents for wastewater treatment, Appl. Surf. Sci. 445 (2018) 30–38.
[8] S. Dong, Y. Cui, Y. Wang, Y. Li, L. Hu, J. Sun, J. Sun, Designing three-dimensional acicular sheaf shaped $BiVO_4$/reduced graphene oxide composites for efficient sunlight-driven photocatalytic degradation of dye wastewater, Chem. Eng. J. 249 (2014) 102–110.
[9] X. Wang, K. Maeda, A. Thomas, K. Takanabe, G. Xin, J.M. Carlsson, K. Domen, M. Antonietti, A metal-free polymeric photocatalyst for hydrogen production from water under visible light, Nat. Mater. 8 (2008) 76–80.
[10] F.K. Kessler, Y. Zheng, D. Schwarz, C. Merschjann, W. Schnick, X. Wang, M.J. Bojdys, Functional carbon nitride materials — design strategies for electrochemical devices, Nat. Rev. Mater. 2 (2017) 17030.
[11] W.-J. Ong, L.-L. Tan, Y.H. Ng, S.-T. Yong, S.-P. Chai, Graphitic carbon nitride (g-C_3N_4)-Based photocatalysts for artificial photosynthesis and environmental remediation: are we a step closer to achieving sustainability? Chem. Rev. 116 (2016) 7159–7329.
[12] S. Cao, J. Low, J. Yu, M. Jaroniec, Polymeric photocatalysts based on graphitic carbon nitride, Adv. Mater. 27 (2015) 2150–2176.
[13] J. Zhang, Y. Chen, X. Wang, Two-dimensional covalent carbon nitride nanosheets: synthesis, functionalization, and applications, Energy Environ. Sci. 8 (2015) 3092–3108.
[14] Y. Zheng, L. Lin, B. Wang, X. Wang, Graphitic carbon nitride polymers toward sustainable photoredox catalysis, Angew. Chem. Int. Ed. 54 (2015) 12868–12884.
[15] Y. Wang, X. Wang, M. Antonietti, Polymeric graphitic carbon nitride as a heterogeneous organocatalyst: from photochemistry to multipurpose catalysis to sustainable chemistry, Angew. Chem. Int. Ed. 51 (2012) 68–89.
[16] K.S. Lakhi, D.-H. Park, K. Al-Bahily, W. Cha, B. Viswanathan, J.-H. Choy, A. Vinu, Mesoporous carbon nitrides: synthesis, functionalization, and applications, Chem. Soc. Rev. 46 (2017) 72–101.
[17] S.J.A. Moniz, S.A. Shevlin, D.J. Martin, Z.-X. Guo, J. Tang, Visible-light driven heterojunction photocatalysts for water splitting - a critical review, Energy Environ. Sci. 8 (2015) 731–759.
[18] X. Dong, F. Cheng, Recent development in exfoliated two-dimensional g-$C3N_4$ nanosheets for photocatalytic applications, J. Mater. Chem. A Mater. Energy Sustain. 3 (2015) 23642–23652.
[19] P. Yang, H. Ou, Y. Fang, X. Wang, A facile steam reforming strategy to delaminate layered carbon nitride semiconductors for photoredox catalysis, Angew. Chem. Int. Ed. 56 (2017) 3992–3996.
[20] Q. Lin, L. Li, S. Liang, M. Liu, J. Bi, L. Wu, Efficient synthesis of monolayer carbon nitride 2D nanosheet with tunable concentration and enhanced visible-light photocatalytic activities, Appl. Catal. B: Environ. 163 (2015) 135–142.
[21] M. Zhu, S. Kim, L. Mao, M. Fujitsuka, J. Zhang, X. Wang, T. Majima, Metal-free photocatalyst for H_2 evolution in visible to near-infrared region: black Phosphorus/Graphitic carbon nitride, J. Am. Chem. Soc. 139 (2017) 13234–13242.
[22] R. Hao, G. Wang, H. Tang, L. Sun, C. Xu, D. Han, Template-free preparation of macro/mesoporous g-C_3N_4/TiO_2 heterojunction photocatalysts with enhanced visible light photocatalytic activity, Appl. Catal. B: Environ. 187 (2016) 47–58.
[23] M.-Y. Ye, Z.-H. Zhao, Z.-F. Hu, L.-Q. Liu, H.-M. Ji, Z.-R. Shen, T.-Y. Ma, 0D/2D heterojunctions of vanadate quantum Dots/Graphitic carbon nitride nanosheets for enhanced visible-light-Driven photocatalysis, Angew. Chem. Int. Ed. 56 (2017) 8407–8411.
[24] Y. Wang, W. Yang, X. Chen, J. Wang, Y. Zhu, Photocatalytic activity enhancement of core-shell structure g-C_3N_4@TiO_2 via controlled ultrathin g-C_3N_4 layer, Appl. Catal. B: Environ. 220 (2018) 337–347.
[25] B. Lin, G. Yang, B. Yang, Y. Zhao, Construction of novel three dimensionally ordered macroporous carbon nitride for highly efficient photocatalytic activity, Appl. Catal. B: Environ. 198 (2016) 276–285.
[26] Z. Tong, D. Yang, Z. Li, Y. Nan, F. Ding, Y. Shen, Z. Jiang, Thylakoid-inspired multishell g-C_3N_4 nanocapsules with enhanced visible-light harvesting and Electron transfer properties for high-efficiency photocatalysis, ACS Nano 11 (2017) 1103–1112.
[27] J. Sun, J. Zhang, M. Zhang, M. Antonietti, X. Fu, X. Wang, Bioinspired hollow semiconductor nanospheres as photosynthetic nanoparticles, Nat. Commun. 3 (2012) 1139.
[28] L. Sun, M. Yang, J. Huang, D. Yu, W. Hong, X. Chen, Freestanding graphitic carbon nitride photonic crystals for enhanced photocatalysis, Adv. Funct. Mater. 26 (2016) 4943–4950.
[29] F. He, G. Chen, J. Miao, Z. Wang, D. Su, S. Liu, W. Cai, L. Zhang, S. Hao, B. Liu, Sulfur-mediated self-templating synthesis of tapered C-PAN/g-C_3N_4 composite nanotubes toward efficient photocatalytic H_2 evolution, ACS Energy Lett. 1 (2016) 969–975.
[30] M. Peer, M. Lusardi, K.F. Jensen, Facile soft-templated synthesis of high-surface area and highly porous carbon nitrides, Chem. Mater. 29 (2017) 1496–1506.
[31] Z. Yang, Y. Zhang, Z. Schnepp, Soft and hard templating of graphitic carbon nitride, J. Mater. Chem. A Mater. Energy Sustain. 3 (2015) 14081–14092.
[32] Z. Chen, S. Lu, Q. Wu, F. He, N. Zhao, C. He, C. Shi, Salt-assisted synthesis of 3D open porous g-C_3N_4 decorated with cyano groups for photocatalytic hydrogen evolution, Nanoscale 10 (2018) 3008–3013.
[33] J. Ran, T.Y. Ma, G. Gao, X.-W. Du, S.Z. Qiao, Porous P-doped graphitic carbon nitride nanosheets for synergistically enhanced visible-light photocatalytic H_2 production, Energy Environ. Sci. 8 (2015) 3708–3717.
[34] Y. Wang, M.K. Bayazit, S.J.A. Moniz, Q. Ruan, C.C. Lau, N. Martsinovich, J. Tang, Linker-controlled polymeric photocatalyst for highly efficient hydrogen evolution from water, Energy Environ. Sci. 10 (2017) 1643–1651.
[35] P. Qiu, C. Xu, H. Chen, F. Jiang, X. Wang, R. Lu, X. Zhang, One step synthesis of oxygen doped porous graphitic carbon nitride with remarkable improvement of photo-oxidation activity: role of oxygen on visible light photocatalytic activity, Appl. Catal. B: Environ. 206 (2017) 319–327.
[36] L. Yang, J. Huang, L. Shi, L. Cao, Q. Yu, Y. Jie, J. Fei, H. Ouyang, J. Ye, A surface modification resultant thermally oxidized porous g-C_3N_4 with enhanced photocatalytic hydrogen production, Appl. Catal. B: Environ. 204 (2017) 335–345.
[37] Z.-F. Huang, J. Song, L. Pan, Z. Wang, X. Zhang, J.-J. Zou, W. Mi, X. Zhang, L. Wang, Carbon nitride with simultaneous porous network and O-doping for efficient solar-energy-driven hydrogen evolution, Nano Energy 12 (2015) 646–656.
[38] H. Yu, R. Shi, Y. Zhao, T. Bian, Y. Zhao, C. Zhou, G.I.N. Waterhouse, L.-Z. Wu, C.-H. Tung, T. Zhang, Alkali-assisted synthesis of nitrogen deficient graphitic carbon nitride with tunable band structures for efficient visible-light-Driven hydrogen evolution, Adv. Mater. 29 (2017) 1605148.
[39] V.W.-h. Lau, D. Klose, H. Kasap, F. Podjaski, M.-C. Pignie, E. Reisner, G. Jeschke, B.V. Lotsch, Dark photocatalysis: storage of solar energy in carbon nitride for time-delayed hydrogen generation, Angew. Chemie Int. Ed. English 56 (2017) 510–514.
[40] G. Liu, G. Zhao, W. Zhou, Y. Liu, H. Pang, H. Zhang, D. Hao, X. Meng, P. Li, T. Kako, J. Ye, In situ bond modulation of graphitic carbon nitride to construct p-n homojunctions for enhanced photocatalytic hydrogen production, Adv. Funct. Mater. 26 (2016) 6822–6829.
[41] V.W.-h. Lau, I. Moudrakovski, T. Botari, S. Weinberger, M.B. Mesch, V. Duppel, J. Senker, V. Blum, B.V. Lotsch, Rational design of carbon nitride photocatalysts by identification of cyanamide defects as catalytically relevant sites, Nat. Commun. 7 (2016) 12165.
[42] D. Zhang, Y. Guo, Z. Zhao, Porous defect-modified graphitic carbon nitride via a facile one-step approach with significantly enhanced photocatalytic hydrogen

evolution under visible light irradiation, Appl. Catal. B: Environ. 226 (2018) 1–9.
[43] H. Ou, P. Yang, L. Lin, M. Anpo, X. Wang, Carbon nitride aerogels for the photoredox conversion of water, Angew. Chem. Int. Ed. 56 (2017) 10905–10910.
[44] P. Niu, L.C. Yin, Y.Q. Yang, G. Liu, H.M. Cheng, Increasing the visible light absorption of graphitic carbon nitride (Melon) photocatalysts by homogeneous self--modification with nitrogen vacancies, Adv. Mater. 26 (2014) 8046–8052.
[45] L. Shi, L. Yang, W. Zhou, Y. Liu, L. Yin, X. Hai, H. Song, J. Ye, Photoassisted construction of holey defective g-C_3N_4 photocatalysts for efficient visible-light-Driven H_2O_2 production, Small 14 (2018) 1703142.
[46] M. Shao, Y. Shao, S. Ding, J. Wang, J. Xu, Y. Qu, X. Zhong, X. Chen, W.F. Ip, N. Wang, B. Xu, X. Shi, X. Wang, H. Pan, Vanadium disulfide decorated graphitic carbon nitride for super-efficient solar-driven hydrogen evolution, Appl. Catal. B: Environ. 237 (2018) 295–301.
[47] M. Shao, Y. Shao, J. Chai, Y. Qu, M. Yang, Z. Wang, M. Yang, W.F. Ip, C.T. Kwok, X. Shi, Z. Lu, S. Wang, X. Wang, H. Pan, Synergistic effect of 2D Ti_2C and g-C_3N_4 for efficient photocatalytic hydrogen production, J. Mater. Chem. A5 (2017) 16748–16756.
[48] Z. Wang, W. Guan, Y. Sun, F. Dong, Y. Zhou, W.-K. Ho, Water-assisted production of honeycomb-like g-C_3N_4 with ultralong carrier lifetime and outstanding photocatalytic activity, Nanoscale 7 (2015) 2471–2479.
[49] X. Wang, X. Wang, J. Zhao, J. Song, J. Wang, R. Ma, J. Ma, Solar light-driven photocatalytic destruction of cyanobacteria by F-Ce-TiO_2/expanded perlite floating composites, Chem. Eng. J. 320 (2017) 253–263.
[50] H. Yan, Soft-templating synthesis of mesoporous graphitic carbon nitride with enhanced photocatalytic H_2 evolution under visible light, Chem. Commun. (Camb.) 48 (2012) 3430–3432.
[51] J. Xiao, Y. Xie, F. Nawaz, Y. Wang, P. Du, H. Cao, Dramatic coupling of visible light with ozone on honeycomb-like porous g-C_3N_4 towards superior oxidation of water pollutants, Appl. Catal. B: Environ. 183 (2016) 417–425.
[52] J. Zhang, S. Hu, Y. Wang, A convenient method to prepare a novel alkali metal sodium doped carbon nitride photocatalyst with a tunable band structure, RSC Adv. 4 (2014) 62912–62919.
[53] J. Jiang, S. Cao, C. Hu, C. Chen, A comparison study of alkali metal-doped g-C_3N_4 for visible-light photocatalytic hydrogen evolution, Chin. J. Catal. 38 (2017) 1981–1989.
[54] L. Jiang, X. Yuan, Y. Pan, J. Liang, G. Zeng, Z. Wu, H. Wang, Doping of graphitic carbon nitride for photocatalysis: a reveiw, Appl. Catal. B: Environ. 217 (2017) 388–406.
[55] J. Zhao, L. Ma, H. Wang, Y. Zhao, J. Zhang, S. Hu, Novel band gap-tunable K-Na co-doped graphitic carbon nitride prepared by molten salt method, Appl. Surf. Sci. 332 (2015) 625–630.
[56] B. Yuan, Z. Chu, G. Li, Z. Jiang, T. Hu, Q. Wang, C. Wang, Water-soluble ribbon-like graphitic carbon nitride (g-C_3N_4): green synthesis, self-assembly and unique optical properties, J. Mater. Chem. C Mater. Opt. Electron. Devices 2 (2014) 8212–8215.
[57] Y. Wang, Y. Li, W. Ju, J. Wang, H. Yao, L. Zhang, J. Wang, Z. Li, Molten salt synthesis of water-dispersible polymeric carbon nitride nanoseaweeds and their application as luminescent probes, Carbon 102 (2016) 477–486.
[58] Y. Li, H. Xu, S. Ouyang, D. Lu, X. Wang, D. Wang, J. Ye, In situ surface alkalinized g-C_3N_4 toward enhancement of photocatalytic H_2 evolution under visible-light irradiation, J. Mater. Chem. A 4 (2016) 2943–2950.
[59] Y. Li, S. Ouyang, H. Xu, X. Wang, Y. Bi, Y. Zhang, J. Ye, Constructing Solid-Gas-Interfacial Fenton reaction over Alkalinized-C_3N_4 photocatalyst to achieve apparent quantum yield of 49% at 420 nm, J. Am. Chem. Soc. 138 (2016) 13289–13297.
[60] F. Guo, J. Chen, M. Zhang, B. Gao, B. Lin, Y. Chen, Deprotonation of g-C_3N_4 with Na ions for efficient nonsacrificial water splitting under visible light, J. Mater. Chem. A 4 (2016) 10806–10809.
[61] X.L. Wang, W.Q. Fang, H.F. Wang, H. Zhang, H. Zhao, Y. Yao, H.G. Yang, Surface hydrogen bonding can enhance photocatalytic H_2 evolution efficiency, J. Mater. Chem. A 1 (2013) 14089–14096.